A Letters Journal Exploring the Frontiers of Physics

November 2019

EPL, **128** (2019) 47002
doi: 10.1209/0295-5075/128/47002

www.epljournal.org

Probing diffusive phase transition in $Ba(Ti_{0.80}Zr_{0.20})O_3$-$0.5(Ba_{0.70}Ca_{0.30})TiO_3$ nanofibers by temperature-dependent piezoelectric force microscopy

Junxi Yu[1,2(a)], Mingkai Tang[1,2(a)], Bi Fu[2(b)], Yong Su[1], Gaokuo Zhong[2(c)], Yun Ou[2], Boyuan Huang[2], Liyu Wei[2], XiangLi Zhong[1], Jinbin Wang[1] and Shuhong Xie[1(d)]

[1] *Key Laboratory of Low Dimensional Materials and Application Technology of Ministry of Education, and School of Materials Science and Engineering - Xiangtan University, Xiangtan, Hunan 411105, China*
[2] *Shenzhen Key Laboratory of Nanobiomechanics, Shenzhen Institutes of Advanced Technology, Chinese Academy of Sciences - Shenzhen, Guangdong 518055, China*

received 29 September 2019; accepted in final form 26 November 2019
published online 24 January 2020

PACS 77.65.-j – Piezoelectricity and electromechanical effects
PACS 77.80.-e – Ferroelectricity and antiferroelectricity
PACS 75.70.Kw – Domain structure (including magnetic bubbles and vortices)

Abstract – $Ba(Ti_{0.80}Zr_{0.20})O_3$-$0.5(Ba_{0.70}Ca_{0.30})TiO_3$ (BTZ-0.5BCT) nanofibers (NFs) demonstrated diffusive phase transition, resulting in an enhanced Curie temperature T_C. As a result, it is scientific significant to probe the variation of ferro/piezoelectricity during such diffusive phase transition region. In this letter, the ferro/piezoelectricity of BTZ-0.5BCT NF was probed by piezoelectric force microscopy (PFM) under a series of temperatures revealing the piezoresponse of BTZ-0.5BCT NF increased with temperatures as the temperature is less than 180 °C. The result shows that the first harmonic piezoresponse initially increased with temperatures, yet two singularities appeared at 120 and 180 °C, and subsequently rapidly decreased to less than room temperature, demonstrating the corresponding ferroelectric transition process was a diffusive phase transition. Such a diffusive phase transition is caused by the discontinuous internal nanostructure of the NF and the size effect of ferro/piezoelectricity originated from the nano-ceramics. More importantly, the principal ferroelectric phase transition of nano-ceramics during such diffusive phase transition region was further quantified by principal component analysis (PCA) study. This indicates that the principal T_C of BTZ-0.5BCT nano-ceramics is around 180 °C, representing the T_C of the whole BTZ-0.5BCT NF. Such a vivid description of the variated ferro/piezoelectricity with temperatures allows to provide a scientific method to quantify diffusive phase transition by PCA study.

Copyright © EPLA, 2020

Ferroelectrics possess the ability of electromechanical coupling that enables to convert mechanical energy into electronical and vice versa, which have a wide range of application in sensor, actuator, energy storage, and communication technology [1–6]. For half a century, $Pb(Zr,Ti)O_3$ (PZT)-based ferroelectrics have had the dominant mainstay of industry because of the superior ferro/piezoelectricity (piezoelectric coefficient, d_{33} = 200–710 pC N^{-1}) [1,4,7–11]. However, very recently, the discovery of lead-free alternatives has become urgent because PZT-based materials have received a global restriction due to the release of toxic PbO during the sintering process [12–14]. For the purpose of discovering lead-free ferroelectrics with superior d_{33} compared to PZT, one representative approach is to make a ferroelectric contain two ferroelectric phases in the proximity of a morphotropic phase boundary (MPB) [1,15–18]. This ferroelectric exhibits an instable polarization state, enabling it to be easily rotated by an external electric field or stress, resulting in a superior piezoelectricity due to the low polarization anisotropy and low energy barrier for lattice distortion [19–21]. Based on this, the lead-free $Ba(Ti_{0.80}Zr_{0.20})O_3$-$x(Ba_{0.70}Ca_{0.30})TiO_3$ (BTZ-0.5BCT) piezoelectric system

(a) These authors contributed equally to this work.
(b) E-mail: bi.fu@siat.ac.cn
(c) E-mail: gk.zhong@siat.ac.cn
(d) E-mail: shxie@xtu.edu.cn

shows surprisingly high d_{33} (620 pC N^{-1}) at optimal composition [15,16,18,22]. As expected, such a high d_{33} of BZT-0.5BCT is comparable to PZT and is higher than a series of other lead-free systems such as (K, Na)NbO_3-based (340–407 pC N^{-1}) [23,24], (Bi, Na)TiO_3-based (135–170 pC N^{-1}) [25], BTS-30BCT (530 pC N^{-1}) [26,27], and BTHf-BCT (550 pC N^{-1}) [28], making it considered as a promising alternative to partly replace PZT-based materials [29,30]. However, its low Curie temperature T_C (93 °C) limits its further applications due to the instability ferroelectric domain at elevated temperature [31]. As a result, it is necessary to make BTZ-0.5BCT not only exhibit superior piezoelectricity but also high T_C.

Ferroelectric nanomaterials exhibit unique physical properties associated with size effect, nanoconfinement effects, and temperature-dependent behaviors [7,17,32–34], especially for the increased T_C originated from the coexistence of ferroelectric phases at high temperature [35,36]. For example, Li reported a very high T_C (220 °C) in electrospun $BaTiO_3$ nanofibers (NFs) by temperature-dependent Raman spectrum, because the reduced grain size leads to larger grain-boundary areas, and further relieved internal stress leads to decreasing the free energy of the ferroelectric phase [37]. Based on this, we previously reported the diffusive phase transition in BTZ-0.5BCT NFs by temperature-dependent Raman spectrum, resulting in a very high T_C (220 °C) because of the coexistence of ferroelectric tetragonal and cubic phase at relatively high temperature [38]. Moreover, Datta reported that the BTZ-0.5BCT nanowire demonstrated increased T_C (up to 300 °C), which is attributed to the volume reduction in the template-grown nanowires that modifies the balance between different structural instabilities [39]. In a word, the enhanced T_C of ferroelectric nanomaterials is commonly attributed to the porous internal nanostructure and size effect of nano-ceramics, resulting in diffusive phase transition. As a result, it is significant to probe the variation of ferro/piezoelectricity in BTZ-0.5BCT NFs during such diffusive phase transition region.

Piezoelectric force microscopy (PFM) is a vigorous tool to probe ferro/piezoelectricity at the nanoscale [17,40–45]. The ferro/piezoelectricity of a single electrospun $BiFeO_3$ NF with dramatically enhanced sensitivity was probed by PFM in our previously report [46]. Moreover, Jalalian reported large d_{33} and ferroelectric domain switching in BTZ-0.5BCT NFs (d_{33} = 180 pm V^{-1}) and thin films (d_{33} = 140 pm V^{-1}) using dual AC resonance tracking (DART)-PFM [31,47]. More importantly, Li reported the thermal variation of microscopically poled P(VDF-TrFE) film under a series of temperatures (27–120 °C) up to the Curie point using PFM, and it can be estimated that the d_{33} ranges from 19.4 to 23 pm V^{-1} [48]. Herein, the ferro/piezoelectricity of BTZ-0.5BCT NFs was probed by temperature-dependent PFM under a series of temperatures ranging from 30 to 220 °C. Moreover, the diffusive phase transition of nano-ceramics was further quantified by principal component analysis (PCA) study [49–52]. This study could help us understand how to quantify the diffusive phase transition of ferroelectric nanomaterials by PCA study.

BTZ-0.5BCT NFs were synthesized by sol-gel electrospinning. All the solvents and raw materials were analytically pure and used without any further purification. First, 1.18 g tetrabutyl titanate ($C_{16}H_{36}O_4Ti$, 99.9%, Alfa, CAS: 5593-70-4), 0.92 g barium acetate ($Ba(CH_3COO)_2$, 98.0%, Alfa, CAS: 543-80-6), 0.21 g zirconium isopropoxide ($C_{15}H_{36}O_5Zr$, 99.0%, Alfa, CAS: 2171-98-4) and 0.06 g calcium acetate ($(C_2H_3O_2)_2Ca$, 99.0%, Alfa, CAS: 5743-26-0) were dissolved into 10 mL acetic acid (CH_3COOH, 99%, Sinopharm, CAS: 64-19-7) on a hot platform of 85 °C with stirring for 12 h. After cooling down to the room temperature, a 10 mL mixture solution of acetyl acetone ($C_5H_8O_2$, 99%, Alfa, CAS: 67-64-1) and 2-methoxyethanol ($C_3H_8O_2$, 99%, Alfa, CAS: 109-86-4) with volume ratio of 5:1.3 was added and kept stirring for 2 h to obtain a 0.2 M BTZ-0.5BCT precursor solution. Next, 2.0 g poly (vinylpyrrolidone) (PVP, K_{30}) was added into a 5 mL BTZ-0.5BCT precursor solution with stirring for 4 h. The obtained precursor solution was loaded into a 10 mL plastic syringe with a stainless steel blunt-tip needle. A high voltage of 12 kV was applied between the needle tip and the aluminium foil current collector with distance of 12 cm. The feeding rate was fixed at 0.3 mL h^{-1}. Finally, the as-spun precursor NFs were dried at 120 °C for 8 h and subsequently annealed at 750 °C for 2 h.

The phase structure was examined by X-ray powder diffraction (XRD, Shimandzu) using a Cu-Kα radiation source (λ = 1.5406 Å). The morphology and microstructure were detected by field-emission scanning electron microscope (FE-SEM, JEOL JSM-7500) and transmission electron microscope (TEM, JEOL ARM-200F) equipped with selected area electron diffraction (SAED). The crystallization and lattice vibration modes were investigated by using Raman spectroscopy (HR800 spectroscope).

The variation of ferro/piezoelectricity during the diffusive phase transition region was further probed by quantitative PFM on an Asylum Research Cypher ES. The sample was placed on a built-in heating stage provided by Asylum Research with temperature ranging from 30 to 220 °C. PFM operated using conductive cantilevers (FMG01/Pt, ∼60 kHz, and ∼3 N m^{-1}) on DART mode near a frequency range of 280–300 kHz, which could enhance the sensitivity of measurement without significant cross-talk between topography and piezoresponse [53]. The first harmonic PFM measurements were carried out by recording amplitude responses with AC voltage between 0.2 and 2.0 V. We scanned 1×1 μm^2 via DART technique with the scanning rate of 0.5 Hz for PFM mappings. A series of PFM response mappings were acquired under different temperatures and the data were post-processed by PCA to enhance signal-to-noise ratio using MATLB. Under PCA, a set of PFM response images (variables) of

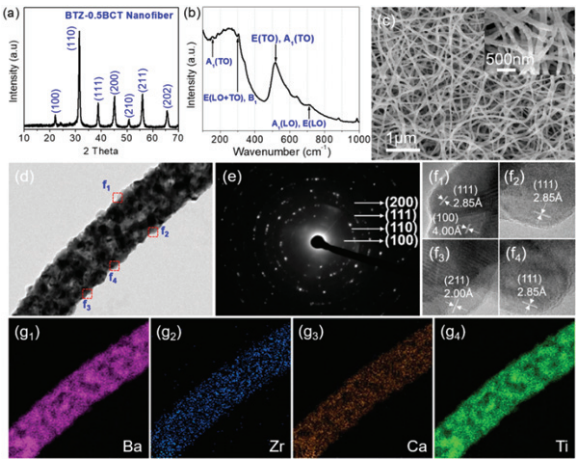

Fig. 1: (a) XRD, (b) Raman spectrum, (c) SEM and (inset) high-magnification SEM image of BTZ-0.5BCT NFs. (d) TEM, (e) SAED pattern of single BTZ-0.5BCT NF. (f_1)–(f_4) HRTEM images obtained from the red boxes of f_1–f_4 in fig. 1(d), respectively. (g_1)–(g_4) TEM element mappings of Ba, Zr, Ca, and Ti elements, respectively.

m-by-n pixels is represented as

$$I_i(\omega_j) = a_{ik} \times v_k(\omega_j),$$

where $a_{ik} = a_k(x, y)$ are position-dependent expansion coefficients known as PCA loadings, $I_i(\omega_j) = I(x, y, \omega_j)$ is the piezoresponse image at discrete temperature ω_j, and v_k are the corresponding eigenvectors. Note that the eigenvectors $v_k(\omega_j)$ and the corresponding eigenvalues λ_k are found from the covariance matrix constructed from piezoresponse mappings with each column corresponding to the reshaped grid points ($i = 1, \ldots, n \times m$) and the rows of covariance matrix representing the experimental variables ($j = 1, \ldots, p$).

Figure 1(a) shows the XRD pattern of BTZ-0.5BCT NFs, revealing a series of diffraction peaks located at 22.1, 31.4, 38.6, 45.2, 51.0, 56.1, and 65.8°, ascribing to the (100), (110), (111), (200), (210), (211), and (202) crystallographic planes of perovskite (JCPDS: 27-0530), respectively [54]. The average crystalline size of BTZ-0.5BCT nanocrystals was calculated from the peaks broadening of (110) reflection using the Scherrer equation [55], which was estimated to be 11.7 nm. Figure 1(b) shows the Raman spectrum of BTZ-0.5BCT NFs. The strong E(LO+TO), B_1 signal at 304.8 cm^{-1}, E(TO), A_1(TO) signal at 518.3 cm^{-1}, and A_1(LO), E(LO) signal at 710.4 cm^{-1} are ascribed to the tetragonal phase, and the A_1(TO) signal at 175 cm^{-1} ascribed to the orthorhombic phase, indicating the coexistence of tetragonal and orthorhombic phase in BTZ-0.5BCT NFs. Figure 1(c) shows the SEM image of BTZ-0.5BCT NF, revealing a nonwoven nanostructure, and the inset high-magnification SEM indicates the ceramic NFs exhibited roughness surface and predominantly 200 nm in diameter. TEM image of single BTZ-0.5BCT NF (fig. 1(d)) reveals that the average size of the nano-ceramic is ∼10 nm. The related SAED pattern in fig. 1(d) displays multiple diffraction rings ascribed to the crystallographic planes of (100), (110), (111), and (200), indicating the polycrystalline nature of BTZ-0.5BCT NFs. HRTEM images of fig. 1(f_1)–(f_4) are obtained from the red boxes of f_1–f_4 in fig. 1(d). These tiny nano-ceramics exhibit interplanar spacing of 2.85, 2.85, 2.00, and 2.85 Å, ascribing to the perovskite crystallographic planes of (111), (111), (211), and (111), respectively. Figure 1(g_1)–(g_4) shows the TEM element mappings of Ba, Zr, Ca, and Ti, respectively. The intensity of Zr and Ca is less than Ba and Ti, revealing a small amount doping of Zr^{2+} and Ca^{2+}. Each of the elements displaying fibrous outline indicates a homogeneously doping of Zr^{2+} and Ca^{2+}. These findings indicate BTZ-0.5BCT NF is composed by nano-ceramics, which is confined into one-dimensional boundary. Such size effect of ferro/piezoelectricity and nanoconfinement effect of one-dimensional boundary are thought to be significant effects on the phase transition of the entire NF.

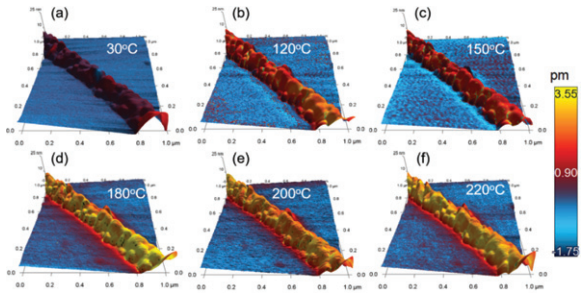

Fig. 2: 3D DART-PFM images of amplitude signals mapping on the surface of single BTZ-0.5BCT NF at (a) 30, (b) 120, (c) 150, (d) 180, (e) 200, and (f) 220 °C.

The variation of ferro/piezoelectricity of a single BTZ-0.5BCT NF was probed by temperature-dependent PFM, as shown in fig. 2. An AFM tip drives an AC voltage of 0.8 V scanning across the surface of BTZ-0.5BCT NF with temperatures of 30, 120, 150, 180, 200, and 220 °C, resulting in the point-to-point amplitude signals, as illustrated in the three-dimensional (3D) 256 × 256 images of fig. 2(a)–(f), respectively. It is obvious that all of the silicon substrates exhibit low-amplitude signals without obviously changing with temperatures. Initially, the BTZ-0.5BCT NF demonstrated piezoelectricity with maximum amplitude of 1.45 pm at 30 °C. Subsequently, the moderate (red domain) and high (yellow domain) amplitude signals alternately appear. Some of the ferroelectric domains span multiple nano-ceramics when the temperature is increased to 120 and 150 °C, because of the strong intergranular interaction [46]. The high piezoresponse domains converge and tend to uniform when the temperature is further increased to 180, 200, and 220 °C, demonstrating the piezoelectricity of the BTZ-0.5BCT NF increases with temperatures.

Figure 3(a) shows the first harmonic piezoresponse of the BTZ-0.5BCT NF at 30, 120, 150, 180, 200, and 220 °C under different drive voltages, and the corresponding

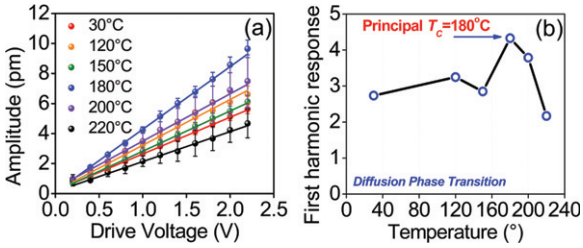

Fig. 3: (a) Amplitude signal *vs.* drive voltage curves, (b) the relationship between the slope of first harmonic piezoresponse and temperatures of 30, 120, 150, 180, 200, and 220 °C.

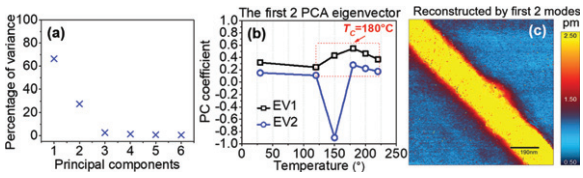

Fig. 4: (a) Eigenvalues *vs.* principal components of phase transition curves, (b) the first two PCA eigenvector of the PCA coefficient *vs.* temperature curve, (c) reconstructed by first 2 modes of the BTZ-0.5BCT NF.

variation of the slope with temperature as shown in fig. 3(b). The initial slope is 2.4 at 30 °C, and is subsequently increased to 3.3 at 120 °C and decreased to 2.8 at 150 °C, it reaches to the maximum value of 4.25 at 180 °C, then rapidly decreases to 2.0 even though the temperature was further increased to 200 °C, which is less than that of 2.4 at room temperature (30 °C). It is obvious that two singularities (∼120 and 180 °C) appear on the slope of first harmonic piezoresponse *vs.* temperature curves, revealing a diffusive phase transition with T_C of ∼120 and 180 °C. Such diffusive phase transition with two singularities is attributed to the fact that different sizes of BTZ-0.5BCT nano-ceramic possess different ferro/piezoelectricity under similar extremal electronical field or strain field [38]. More importantly, the principal ferroelectric phase transition associated with the size effect of nano-ceramics during such diffusive phase transition region was further investigated by PCA study.

The PCA eigenvalues drop rapidly after the second one as shown in fig. 4(a) indicates the first two components are important and contain most of the information and the dominant physical properties of the material. The subsequent four components are similar and tend to zero, ascribing to the low noise signals in the environment during the PFM probing process [49]. The first two eigenvectors capture the average spectrum of data as a function of discrete set of temperature, as shown in fig. 4(b), wherein the first eigenvector exhibits diffusive phase transition during the temperature ranging from 120 to 220 °C with a peak of 180 °C. The second eigenvector, presenting a trough at 150 °C, coincides with the observation in fig. 3(b). Compared to the first eigenvector, the second eigenvector takes only about 27% variance of data, demonstrating the dominant diffusive phase transition at 180 °C. The component image is reconstructed by the first two PCA loadings in fig. 4(c), revealing enhanced signal-to-noise ratio. The PCA study reveals the principal tetragonal-to-cubic ferroelectric phase transition of nano-ceramics during the diffusive phase transition region, indicating that the principal T_C of BTZ-0.5BCT NF is ∼180 °C, which is more than its bulk material of 93 °C [15]. BTZ-0.5BCT NF exhibits diffusive phase transition because of the porous internal nanostructure and size effect of ferro/piezoelectricity [38]. High-temperature solid-state reaction synthesized BTZ-0.5BCT solid solution exhibits compact internal structure with the micron-level ferroelectric domain, demonstrating diffusionless phase transition, which is different from its nanomaterials [15,22].

In summary, the ferro/piezoelectricity of BTZ-0.5BCT NFs were probed by temperature-dependent PFM with temperatures ranging from 30 to 220 °C, revealing the piezoresponse increases with temperature. The first harmonic piezoresponse increases with temperature, yet there are two singularities at 120 and 180 °C, and it subsequently rapidly decreases, demonstrating a diffusive phase transition. Such a diffusive phase transition is attributed to the porous internal nanostructure of the NF and the size effect of the ferro/piezoelectricity originated from the nano-ceramics. Moreover, the principal ferroelectric phase transition of the nano-ceramics can be quantified by PCA study, indicating that the principal T_C of nano-ceramics is ∼180 °C, representing the T_C of the whole BTZ-0.5BCT NF. These findings help us understand how to quantify the diffusive phase transition of ferroelectric nanomaterials by PCA study.

* * *

We acknowledge the National Key Research and Development Program of China (2016YFA0201001), National Natural Science Foundation of China (11802318, 11627801, 11472236, 51902337 and 51702351), Pearl River Talent Plan (2017GC010051), National Science Foundation of Guangdong Province (2017A030310433), Innovation Team of Hunan Province (2018RS3091), Shenzhen Science and Technology Innovation Committee (JCYJ20170818155200084, JCYJ20170818160503855, and JCYJ20170413152832151).

REFERENCES

[1] Li J. Y., Rogan R. C., Üstündag E. *et al.*, *Nat. Mater.*, **4** (2005) 776.
[2] You Y. M., Liao W. Q., Zhao D. *et al.*, *Science*, **357** (2017) 306.
[3] Hill N. A., *J. Phys. Chem. B*, **104** (2000) 6694.
[4] Auciello O., Scott J. F. and Ramesh R., *Phys. Today*, **51**, issue No. 7 (1998) 22.

[5] Ping W., Liu W. and Li S., *Ceram. Int.*, **45** (2019) 11388.
[6] Zhong G. K., Bitla Y., Wang J. B. *et al.*, *Acta Mater.*, **145** (2018) 488.
[7] Espinosa H. D., Bernal R. A. and Minary-Jolandan M., *Adv. Mater. Int.*, **24** (2012) 4656.
[8] Zhou Z., Tang H. and Sodano H. A., *Adv. Mater.*, **26** (2014) 7547.
[9] Xie Y., Ou Y., Ma F. Y. *et al.*, *Nanosci. Nanotechnol. Lett.*, **5** (2013) 546.
[10] Xie S. H., Li J. Y., Qiao Y. *et al.*, *Appl. Phys. Lett.*, **92** (2008) 062901.
[11] Xie S. H., Liu Y. M., Ou Y. *et al.*, *J. Appl. Phys.*, **112** (2012) 074110.
[12] Wu W., Cheng L., Bai S. *et al.*, *J. Mater. Chem. A*, **1** (2013) 7332.
[13] Baek C., Yun J. H., Wang J. E. *et al.*, *Nanoscale*, **8** (2016) 17632.
[14] Rödel J., Jo W., Seifert K. T. P. *et al.*, *J. Am. Ceram. Soc.*, **92** (2009) 1153.
[15] Liu W. and Ren X., *Phys. Rev. Lett.*, **103** (2009) 257602.
[16] Liu Y. Y. and Li J. Y., *Phys. Rev. B*, **84** (2011) 132104.
[17] Liu Y. Y., Zhu Z. X., Li J. F. *et al.*, *Mech. Mater.*, **42** (2010) 816.
[18] Peng J. L., Li Q., Shan D. L. *et al.*, *J. Appl. Phys.*, **119** (2016) 204103.
[19] Gao J., Hu X., Zhang L. *et al.*, *Appl. Phys. Lett.*, **104** (2014) 252909.
[20] Keeble D. S., Benabdallah F., Thomas P. A. *et al.*, *Appl. Phys. Lett.*, **102** (2013) 092903.
[21] Gao J., Xue D., Wang Y. *et al.*, *Appl. Phys. Lett.*, **99** (2011) 092901.
[22] Peng J., Shan D., Liu Y. *et al.*, *npj Comput. Mater.*, **4** (2018) 66.
[23] Tao H., Wu J., Xiao D. *et al.*, *ACS Appl. Mater. Int.*, **6** (2014) 20358.
[24] Jalalian A. and Grishin A. M., *Appl. Phys. Lett.*, **100** (2012) 012904.
[25] Li T., Lou X., Ke X. *et al.*, *Acta Mater.*, **128** (2017) 337.
[26] Zhu L.-F., Zhang B.-P., Zhao X.-K. *et al.*, *Appl. Phys. Lett.*, **103** (2013) 072905.
[27] Xue D., Zhou Y., Bao H. *et al.*, *Appl. Phys. Lett.*, **99** (2011) 122901.
[28] Zhou C., Liu W., Xue D. *et al.*, *Appl. Phys. Lett.*, **100** (2012) 222910.
[29] Yuan M., Cheng L., Xu Q. *et al.*, *Adv. Mater.*, **26** (2014) 7432.
[30] Praveen J. P., Kumar K., James A. R. *et al.*, *Curr. Appl. Phys.*, **14** (2014) 396.
[31] Jalalian A., Grishin A. M., Wang X. L. *et al.*, *Appl. Phys. Lett.*, **104** (2014) 103112.
[32] Rørvik P. M., Grande T. and Einarsrud M.-A., *Adv. Mater.*, **23** (2011) 4007.
[33] Nuraje N. and Su K., *Nanoscale*, **5** (2013) 8752.
[34] Zhang Y., Hong J., Liu B. *et al.*, *Nanotechnology*, **20** (2009) 405703.
[35] Bjørnetun Haugen A., Forrester J. S., Damjanovic D. *et al.*, *J. Appl. Phys.*, **113** (2013) 014103.
[36] Lee M. H., Kim D. J., Park J. S. *et al.*, *Adv. Mater.*, **27** (2015) 6976.
[37] Li H., Wu H., Lin D. *et al.*, *J. Am. Ceram. Soc.*, **92** (2009) 2162.
[38] Fu B., Yang Y., Gao K. *et al.*, *Appl. Phys. Lett.*, **107** (2015) 042903.
[39] Datta A., Sanchez-Jimenez P. E., Al Orabi R. A. R. *et al.*, *Adv. Funct. Mater.*, **27** (2017) 1701169.
[40] Li J., Li J.-F., Yu Q. *et al.*, *J. Materiomics*, **1** (2015) 3.
[41] Yu J., Esfahani E. N., Zhu Q. *et al.*, *J. Appl. Phys.*, **123** (2018) 115104.
[42] Yu Q., Li J.-F., Sun W. *et al.*, *Appl. Phys. Lett.*, **104** (2014) 012908.
[43] Chen Q. N., Ou Y., Ma F. *et al.*, *Appl. Phys. Lett.*, **104** (2014) 242907.
[44] Liu Y. Y., Seidel J. and Li J. Y., *Nat. Sci. Rev.*, **6** (2019) 626.
[45] Fu B., Lu R. E., Gao K. *et al.*, *EPL*, **111** (2015) 17007.
[46] Xie S., Gannepalli A., Chen Q. N. *et al.*, *Nanoscale*, **4** (2012) 408.
[47] Rodriguez B. J., Callahan C., Kalinin S. V. *et al.*, *Nanotechnology*, **18** (2007) 475504.
[48] Liu Y., Xie S., Liu X. *et al.*, *J. Appl. Phys.*, **110** (2011) 052008.
[49] Xia G., Huang B., Zhang Y. *et al.*, *Adv. Mater.*, **31** (2019) e1902870.
[50] Jiang P., Huang B., Wei L. *et al.*, *Nanotechnology*, **30** (2019) 205703.
[51] Huang B., Esfahani E. N. and Li J., *Nat. Sci. Rev.*, **6** (2019) 55.
[52] Li J., Huang B., Nasr Esfahani E. *et al.*, *npj Quantum Mater.*, **2** (2017) 56.
[53] Fu B., Lu R., Gao K. *et al.*, *EPL*, **112** (2015) 27002.
[54] Chi Q., Ma T., Zhang Y. *et al.*, *J. Mater. Chem. A*, **5** (2017) 16757.
[55] Alexander L. and Klug H. P., *J. Appl. Phys.*, **21** (1950) 137.